Chapter 2

Two dimensional amide linked porous polymer as organocatalyst to promote selective oxidation reactions

2.1 Abstract

This chapter describes the synthesis of an amide linkage porous organic polymer with [3+2] structure motif via the condensation of 1,3,5-benzenetricarbonyl trichloride and *p*-phenylenediamine. The synthesized mesoporous 2D organic polymer is chemically and thermally stable exhibiting continuous conjugation of π-electronic system. This polymeric network solid displays excellent catalytic activity towards selective oxidation reactions manifested by the conjugated π-cloud and amide functionality. This chapter demonstrates the catalytic activity of polymeric material in reaction of various substituted benzyl alcohols to their corresponding aldehydes. This is one of the rare cases of any organic polymeric material acting as an organic catalyst. A free radical reaction mechanism is proposed for the reaction supported by experimental study and computational analysis.

2.2 Introduction

Covalent porous organic polymer materials represent the periodic ordering of organic building units' ensemble via covalent bonds [1-3]. The topological design of these building units considered for the construction of POPs defines the polymers shape, size, pore volumes and functionality in its crystal lattice [4]. The architecture of these polymers are entirely composed of lighter elements viz., B, C, N, O, etc. interconnected through C–C, C–O, B–O, C–N, etc. bonds. The physical properties of these porous polymeric networks are exaggerated by the interlayer planarization between the polymeric sheets [4,5]. It includes reduce in band gap, improvement in photocatalytic activity, crystallinity, porosity, etc. of the polymer. The planar conformation of the network is triggered by the presence of π-cloud delocalization over the polymeric sheets. Existence of delocalized π-cloud also renders extra stability toward the materials. These stable porous polymeric materials with tailor-made physical and chemical properties exhibit wonderful applications in gas storage [6-8], conduction [5, 9,10], energy storage and conversion [11-13], biomedicine [14,15] and recently applied to promote catalysis [16,17].

In catalysis, the imine linkage POPs have been widely investigated. To mention a few, the Suzuki-Miyaura coupling [18], Mizoroki–Heck [19], Knoevenagel condensation [20], Michael addition [21] and few acidic-basic cascade reactions [22,23], etc. have been reported where POPs have been used for carrying out the respective organic transformation reaction. The superior activity of Pd incorporated 2D crystalline POP in Suzuki-Miyaura coupling is due to its well-organized access to the catalytically active sites and fast diffusion of the reactants/products from the pores. The Knoevenagel condensation reaction is accomplish by a 3D microporous crystalline POP that acts as a base to catalyze the reaction. Banerjee and co-workers used imine linked 2D porous polymer as support matrix for immobilization of Au(0) nanoparticles and employed as heterogeneous catalyst with fine dispersion of Au nanoparticles for the reduction of nitrophenol [24]. POP with π-electronic cloud has also been examined as metal free catalytic support for Diels–Alder reaction [25]. In addition, the asymmetric Diels–Alder reaction has successively performed by the application of metal free chiral POP with good efficiency and enantioselectivity [26]. This reaction was facilitated upon existence of chiral building blocks in POP synthesis. The porous framework comprising of cobalt porphyrins have been identified lately as an efficient catalyst for the reduction of CO_2, a gas responsible for global warming [27]. Thus, POPs exhibit excellent support matrix for transition metal incorporation in catalysis. Literature evidences the utility of POPs as metal catalyst carrier in biorefinery and biodiesel production from renewable sources [28-33]. These polymeric networks prove as organic catalyst in accomplishing its potent applications as heterogeneous catalyst in organic transformation reactions. In this context, the present mesoporous organic polymer synthesized from 1,3,5-benzenetricarbonyl trichloride (BzCl) and *p*-phenylenediamine (PD) following [3+2] structure motif (hereafter POP-Am, Scheme 2.1, detail synthetic procedures in experimental section) is a rare finding to address the issues of metal free catalyst. It has been utilized as heterogeneous catalyst with high stability and recyclability for selective oxidation of benzyl alcohols [34]. The reaction has been elucidated by moderate to better yields depending on the nature of the substituent's (Table 2.1).

Classical method of synthesis of aldehydes in laboratories and also in industries is an oxidative process which carried out in the presence of a metal catalyst. Corey's Reagent [35], Swern oxidation [36], Dess-Martin reaction [37], etc. are such common methods which are not sustainable environmentally. In addition, such process tends to the

formation of over oxidized product viz. carboxylic acid. Thus in the awareness of 21st century, the conventional industrial synthetic processes were detrimental to the environment. It led to a movement towards reshaping the science of organic synthetic chemistry. In relation to it, the selective oxidation of benzyl alcohols to benzaldehyde with environmentally benign method is of nature demand. Notably, literature reveals the use of metal (such as Au, Pd, Pt, Ru, Cu, etc.) supported species as catalyst for oxidation of alcohols [38-44]. These metal catalysts have vacant coordination sites providing opportunities for water molecules to coordinate. As a consequence, the deactivation of such metals in oxidation process is of high concern. Thus, the existence of toxic traces of heavy metals cannot be neglected in the products. Needless to mention that it is highly desirable to develop environment friendly new oxidization protocols that remain a great challenge. Recent reports stated the use of metal free oxidants such as a mixture of TEMPO/Br_2/$NaNO_2$ or TEMPO/HCl/$NaNO_2$ in catalytic amounts, P- or N- doped porous carbon and/or graphene for selective aerobic oxidation of benzylic alcohols [45-47]. The POP-Am addresses such emerges in terms of a novel metal free and selective oxidation. The reaction was tested in presence of *tert*-butyl hydrogen peroxide (TBHP) as oxidant and compared with hydrogen peroxide (H_2O_2). To establish the generality of the newly developed synthetic route for selective oxidation, substrates with different functional groups like –Cl, –Br, –NO_2, –OCH_3, –CH_3, –H, etc. have been studied.

The extended π-cloud delocalization via -CONH- group over the 2D molecular sheets of POP-Am triggers the porous structure in nearly planar conformation. The interlayer planarization amplifies the physical properties of the material thereby improving its catalytic activity. In addition, the π-cloud delocalization also provides stability to the material. With these possibilities, POP-Am has been synthesized and exploited its π-electronic bed and -CONH- group as a support for oxidation reaction by initiating and stabilizing reaction intermediates and products. More precisely, interaction of reactants with -CONH- group and π-cloud delocalization affect reaction kinetics by changing activation barrier supported by computation. Therefore, it is has been anticipated that the study presented in this chapter would open a novel approach to the structural and functional design of POPs, particularly in heterogeneous metal free catalysis.

2.3 Results and discussion

2.3.1 Synthesis of 2D porous polymeric framework POP-Am

A new two-dimensional amide linked organic porous polymeric network (POP-Am) has been synthesized from 1,3,5-benzenetricarbonyl trichloride (BzCl) and *p*-phenylenediamine (PD) following [3+2] structure motif (Scheme 2.1). The carboxamide moiety in the structure is identified as the H-bonding interaction site and can be exploited for gas adsorption studies. The adsorption behavior of this material increases due to orientation of amide C=O and N−H towards the pores. This in turn enhances hydrogen bonding and/or van der Waals interaction propensity with the guest (i.e. small sized gas, water and solvent molecules). Also, the availability of π-electrons propagated by amide group in the polymeric framework provides opportunity for POP-Am to be explored as support matrix in carrying out organic reactions.

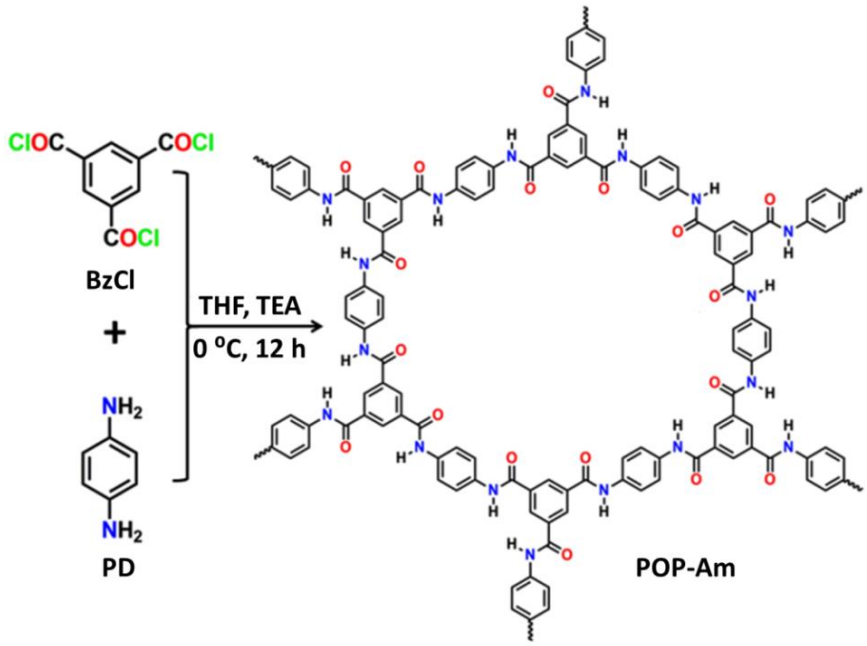

Scheme 2.1 Schematic representation of POP-Am synthesis from BzCl (1,3,5-benzenetricarbonyl trichloride) and PD (*p*-phenylenediamine).

2.3.2 Characterization of POP-Am

The preliminary information about the formation of a specific functional group in an organic molecule could be gathered from the FT-IR spectroscopy. The diminution of N–H stretching frequency of amine at around 3400 cm^{-1} and C=O stretching frequency of carbonyl chloride at around 1754 cm^{-1} assigns the conversion of acyl chloride into carboxamide. The appearance of strong absorption band in the range 1690–1630 cm^{-1}

encircled with dotted black in Figure 2.1a stands for amide $\nu_{C=O}$. This provides the clear information about the condensation of BzCl and PD affording the desired amide functionality in the polymeric framework POP-Am.

Further information about the crystallinity of POP-Am is provided by recording the powder X-ray diffraction (PXRD) pattern. The intense peak at 2θ = ~3° and broad peak within 20°–35° in the PXRD (Figure 2.1b) indicates reasonable crystallinity of the material with an ordered layer structure.

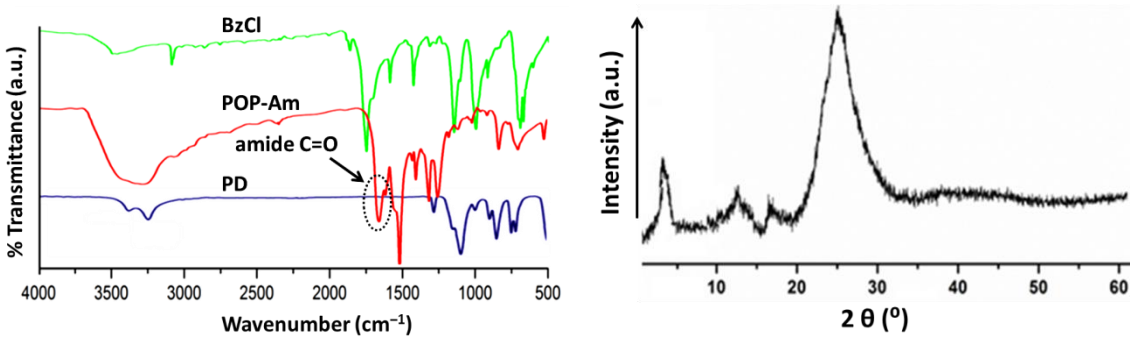

(a) (b)

Figure 2.1 Comparison of FT-IR spectra of building units and the synthesized POP-Am reveals the formation of carboxamide (amide C=O in circle) linkage in POP-Am (a) and PXRD pattern evidencing microcrystalline nature of POP-Am having an ordered layered structure (b).

In general, the amide functionality is consistent with hydration and it is the C=O rather than the N−H that is being hydrated because of excellent hydrogen bonding capability of both as a donor and as an acceptor. The TGA trace of the POP-Am kept under relative humidity (RH) of 92 % for 10 days showed substantial weight loss (up to 28%) under 100 °C. It suggests that the material is moisture sensitive. The synthesized POP-Am experiences a significant weight loss at temperature range 200 to 250 °C and is due to the trapping of guest molecules inside the cavities. However, the POP-Am activated at 250 °C for 1 h discloses the guest free POP-Am stable up to ~400 °C (Figure 2.2a).

POP-Am is found stable and insoluble in aqueous medium, common laboratory solvents, strong acids and bases. Its stability is examined by treating the polymeric material with respective solvent medium and recording the IR spectra. Appearance of alike C=O stretching frequency range in all cases (between red strip in Figure 2.2b) reveals its

chemical stability. The higher stability of POP-Am is reasoned due to the presence of heat resistance carboxamide linkage in its structure.

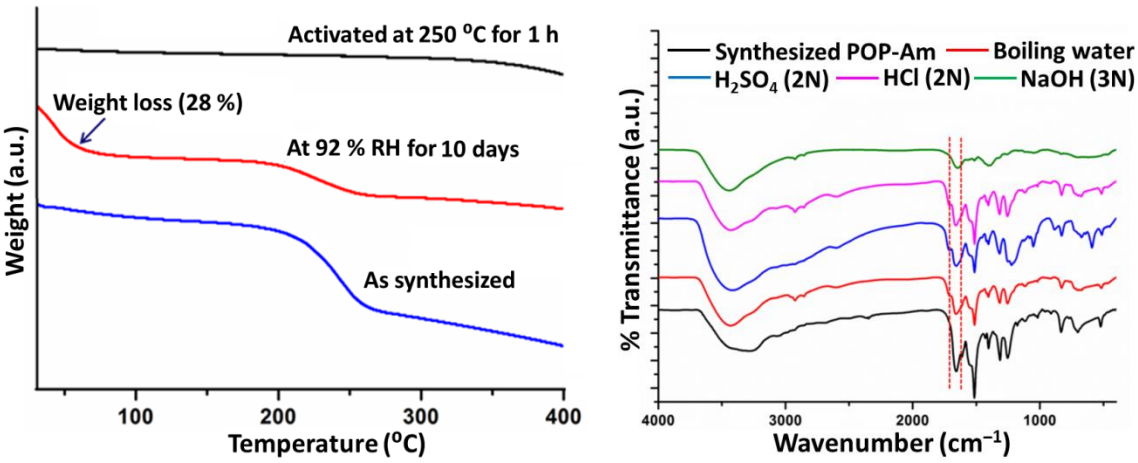

(a) (b)

Figure 2.2 TGA plot displaying the stability of POP-Am at various conditions (a) and FT-IR spectra displaying the stability of POP-Am at various environments (b).

Since POP-Am is insoluble in common laboratory solvents the solid state NMR (ssNMR) technique was employed to understand the chemical environment in it. The analysis of the spectra and relaxation parameters of cross polarization magic angle spinning (CP-MAS) ^{13}C ssNMR indicates a strong absorption of chemical shift at 165 ppm indicating the presence of carboxamide carbonyl group (Figure 2.3). The chemical shift value of other aromatic carbons appears at 121, 122, 127 and 135 ppm respectively.

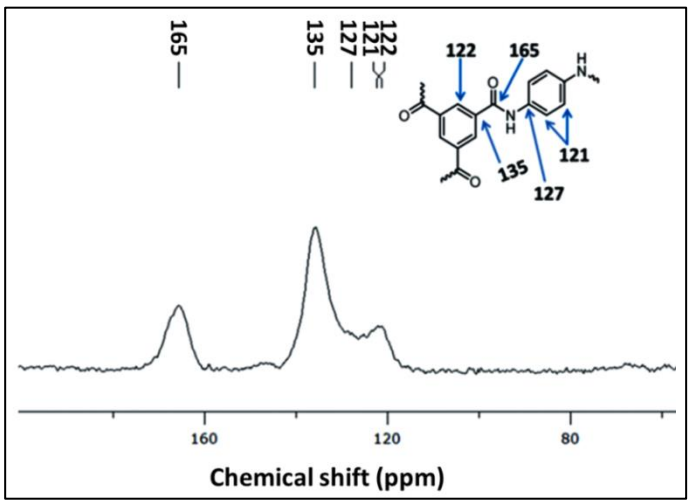

Figure 2.3 The cross polarization magic angle spinning (CP-MAS) ^{13}C-NMR spectrum rendering the chemical environment of POP-Am.

The structural integrity of the material ensures adsorption of gases like N_2, CO, CO_2 etc. as they can weakly bind to the carboxamide moiety. The N_2 adsorption and desorption isotherms of POP-Am was recorded at 77 K to examine the porosity behavior. Prior to the experiment the material was activated and degasified at 120 °C to ensure the pores to be guest free. The nitrogen uptake isotherm (Figure 2.4a) revealed POP-Am as mesoporous material exhibiting type-II adsorption isotherm with pore size of 2.24 nm. From Brunauer-Emmet-Teller (BET) isotherm the surface area of POP-Am is calculated to be 65 m^2g^{-1} and the surface area plot have been depicted in Figure 2.4b. Jong et al. reported isotherm with similar capillary condensation for mesoporous zeolite [48]. Further, they observed hysteresis loop indicating the mesopores with pore closure at 0.45 relative pressures. Whereas in POP-Am, the closure is at about 0.6 relative pressure implying that pores get blocked only thereafter.

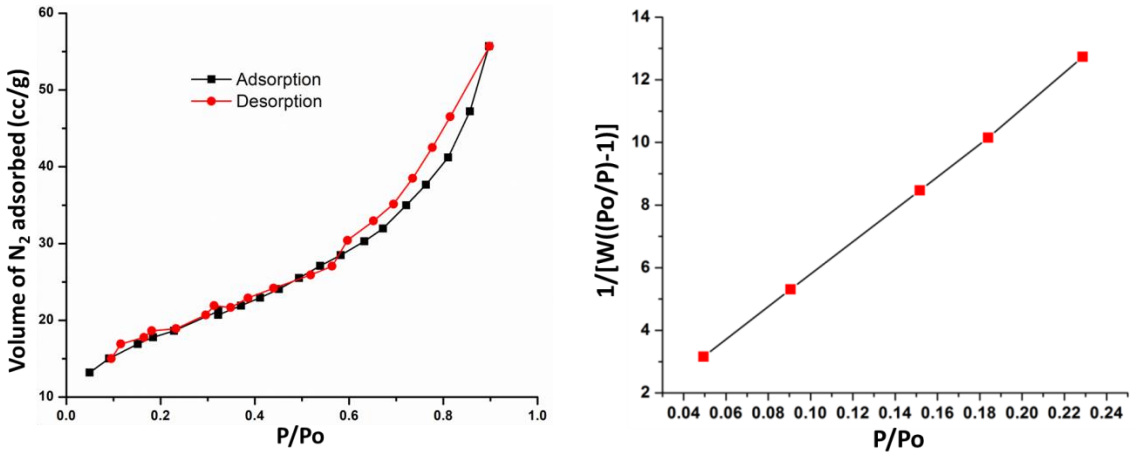

(a) (b)

Figure 2.4 Nitrogen adsorption-desorption isotherm at 77 K displaying the type-II adsorption isotherm of POP-Am (a) and its BET surface area plot from which the surface is calculated to be 65 m^2g^{-1} (b).

In order to draw further information about the structure and pore size of POP-Am, the expected structure is drawn and optimized using DMol3 [49] in Material Studio 7.0 package. However, only a single ring of POP-Am with anti-amide conformation has been considered for the optimization by fixing the extended networking site of the building unit via hydrogen atom. The optimized structure (Figure 2.5) shows a nearly planar conformation with pore radius of 2.0 nm that resembles with experimental value (2.2 nm) extracted from BET analysis. Observed low surface area could be because of the random orientation and/or interpenetration of outgrowth arms via the pores.

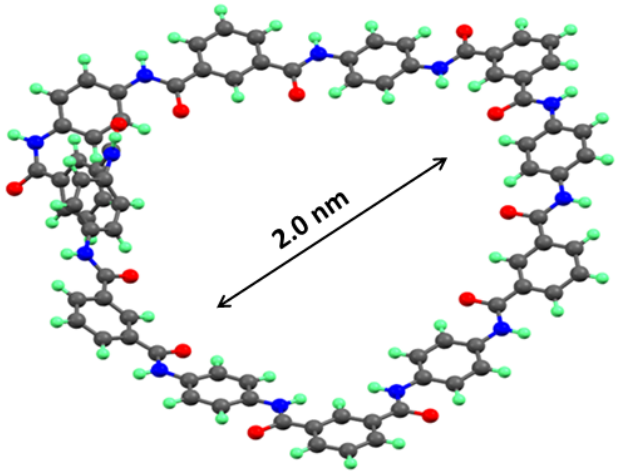

Figure 2.5 Structure optimization of a single ring in POP-Am by fixing the extended networking site of the polymer via hydrogen atom displaying nearly planar shape of POP-Am.

The surface morphology of the material is investigated using scanning electron microscopy (SEM) and high resolution transmission microscopy (HR-TEM). The SEM images showed agglomeration of the spherical particles (Figure 2.6a,b), whereas TEM images evidenced the interconnection, continuous and extended porous network structure (Figure 2.6c,d).

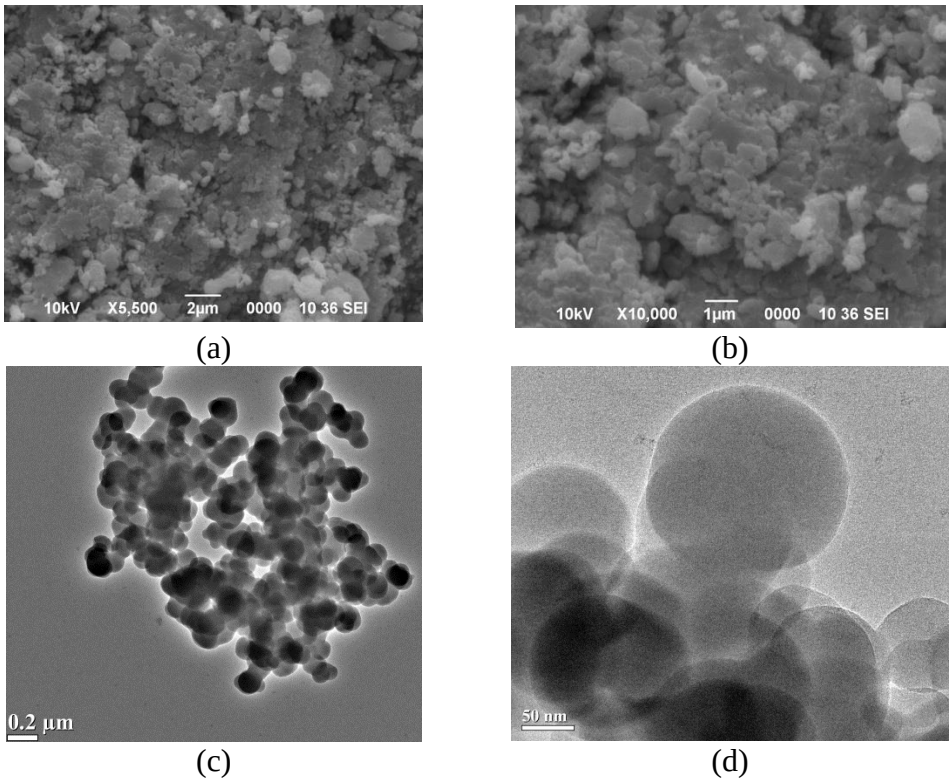

Figure 2.6 SEM images (a,b) and HR-TEM images (c,b) of POP-Am.

2.3.3 POP-Am as organic catalyst in selective oxidation of benzyl alcohols

Use of POP as conducting material has been studied by preparing crystalline POPs with ordered π-columns. The columnar π-wall elicits significant electronic coupling allowing delocalization of π-cloud which facilitates charge transport through the π-channels [50]. To understand conduction behavior of POP-Am, electronic absorption spectroscopy was performed to evaluate the π-electronic functions. For comparison *N*-phenyl-benzamide was synthesized and considered as the carboxamide monomer unit which exhibited an absorption band at ~285 nm. Whereas, the POP-Am exhibited a red-shift of band gap difference 1.0 eV (band at ~356 nm, Figure 2.7) establishing 2D extended π-cloud delocalization over the ordered framework structure. Therefore, probability increases for easy electronic transition that could promote catalysis. The characterized POP-Am with continuous π-conjugation is employed as a metal free heterogeneous catalyst for selective oxidation of benzyl alcohols using TBHP as oxidant to the corresponding benzaldehydes (Scheme 2.2). The reaction condition is optimizing at ~14 h with up to 95% yield and 100% selectivity (Table 2.1). A set of reactions is performed at different temperatures to understand the threshold temperature of the reaction and found to be 60 °C. To understand the further catalytic scope of POP-Am benzyl alcohols with various substituents is considered for the oxidation (Table 2.1). The final products are further characterized by ^{1}H- and ^{13}C-NMR spectroscopy and GC-MS chromatographic technique.

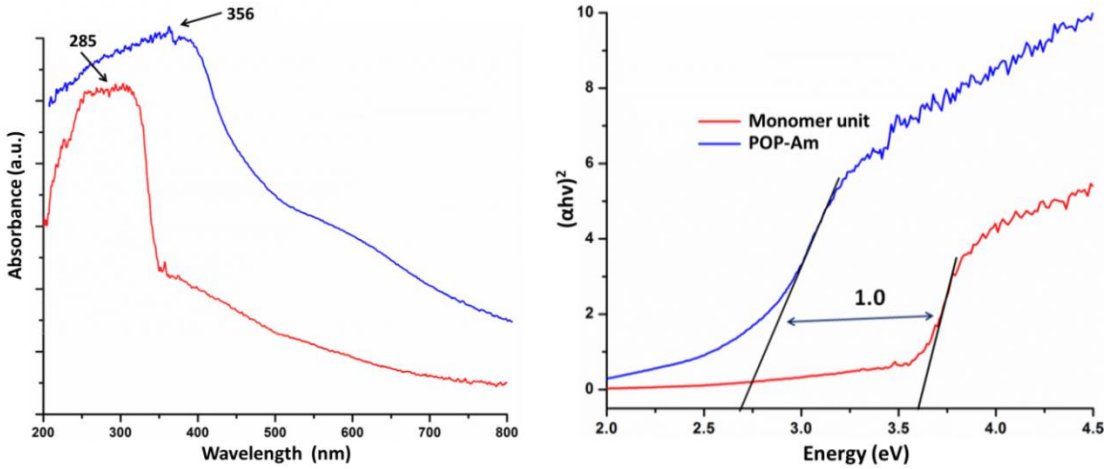

Figure 2.7 Solid UV-Vis spectra (a) and the difference in energy band gap between (b) POP-Am (blue) and its monomeric unit, *N*-phenyl benzamide (red).

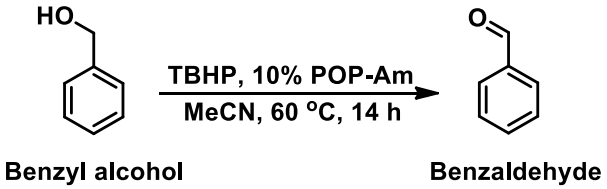

Scheme 2.2 Selective oxidation of benzyl alcohol to benzaldehyde using metal free catalyst POP-Am.

Table 2.1 Oxidation of benzyl alcohols and it derivatives using POP-Am as catalyst

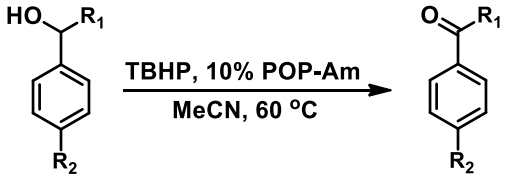

Entry	R_1	R_2	Time (h)	Yield (%)	Selectivity (%)
1.	H	H	14	63	100
2.	Cl	H	14	44	100
3	Br	H	14	47	100
4.	NO_2	H	14	>95	100
5.	Me	H	14	92	100
6	OMe	H	14	78	100
7.	H	Phenyl	10	80	100
8.	H	Me	10	54	100
	Reactant		Time	Product	
9.	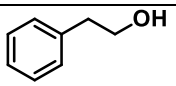		14	No reaction	
10	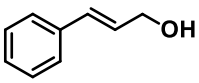		14	No reaction	
11.	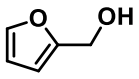		14	No reaction	
12.	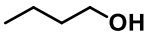		14	No reaction	

However, no product formation is detected when the reaction was progressing in absence of catalyst and in presence of the TBHP (Scheme 2.3) as revealed by GC-MS

chromatogram. This indicates the role of POP-Am in the successful oxidation of benzyl alcohols.

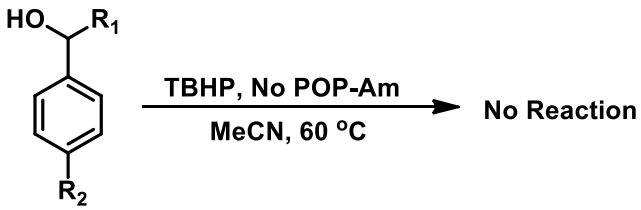

Scheme 2.3 Oxidation of benzyl alcohols does not proceed in absence of POP-Am.

The identical reactions at optimal condition are further carried out using H_2O_2 as oxidant instead of TBHP. Negligible product formation was observed in few reactions, while it does not proceed at all in others. Possibly the stronger leaching ability reduces the efficiency of H_2O_2. Essentially TBHP forms a more stable radical species than the corresponding H_2O_2 homologue but bulkier substrate. Hence, it restricts hydration propensity and free diffusion of the TBHP from the catalyst. Nonetheless, H_2O_2 is not easily miscible with non-polar solvents and cannot be used under anhydrous condition. As a result, it shows differences in substrate reactivity (Table 2.2) and allows the catalytic process to continue with TBHP, while being relatively expensive.

Table 2.2 Screening of oxidants in selective oxidation of benzyl alcohols in table 2.1 to the corresponding benzaldehydes, TBHP has been found to be better in terms of yield

Entry	R_1	R_2	Time (h)	Oxidants	Yield (%)
1.	H	H	14	TBHP	63
				H_2O_2	ND
2.	Cl	H	14	TBHP	44
				H_2O_2	Trace
3	Br	H	14	TBHP	47
				H_2O_2	Trace
4.	NO_2	H	14	TBHP	>95
				H_2O_2	Trace
5.	Me	H	14	TBHP	92
				H_2O_2	Trace
6.	OMe	H	14	TBHP	78

				H_2O_2	Trace
7.	H	Phenyl	10	TBHP	80
				H_2O_2	ND
8.	H	Me	10	TBHP	54
				H_2O_2	ND

*ND: Not detected in GC-MS analysis.

In order to gather further insight of the mechanistic route towards the formation of benzaldehydes, the oxidation is carried out in presence of TEMPO, a popular free radical scavenger (Scheme 2.4). Interestingly the reaction freezes, further confirming a free radical mechanism for the reaction. This signifies the role of POP-Am in initiating the reaction via the formation of *tert*-butoxy free radicals.

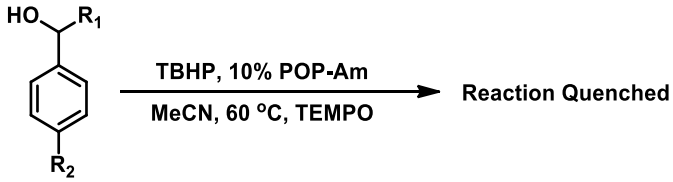

Scheme 2.4 Oxidation of benzyl alcohols to the corresponding carbonyl compounds freezes while performing the reactions in presence of free radical scavenger (TEMPO) thereby indicating the formation of free radicals during the reaction process.

To generalize this approach using POP-Am as metal free catalyst for selective oxidation of benzyl alcohols, polyurethane composed of organic units joined by carbamate was chosen as the heterogeneous organocatalyst. Carbamate offers two advantages, i.e. presence of amide functional group and ineffective π- conjugation. Under same reaction conditions in Table 2.1, the progress of the reaction is found very slow with trace to null amount of product formation (Table 2.3). Therefore, it is speculated that the reaction has been initiated by amide functionality as in the case of POP-Am. This is followed by stabilization of generated free radicals of TBHP through hydrogen bonds. In addition, collapse of extended π-conjugation in polyurethane might lead to raise in band gap energies. It in turn disfavors electron cloud to assist the oxidation process. As a consequence, the easy electronic transition to the polymeric surface declines. Eventually the interaction energy of hydroxyl radicals with π-cloud via directional O−H···π interaction decreases thereby lowering the stability of radicals on the catalyst surface.

Table 2.3 Comparing the catalytic activity of POP-Am and polyurethane both having different monomeric unit in presence of TBHP as oxidant in oxidation of alcohols in Table 2.1

Entry	R_1	R_2	Time (h)	Catalysts	Yield (%)
1.	H	H	14	POP-Am	63
				Polyurethane	5
2.	Cl	H	14	POP-Am	44
				Polyurethane	Trace
3	Br	H	14	POP-Am	47
				Polyurethane	2
4.	NO_2	H	14	POP-Am	>95
				Polyurethane	3
5.	Me	H	14	POP-Am	92
				Polyurethane	5
6.	OMe	H	14	POP-Am	78
				Polyurethane	~2
7.	H	Phenyl	10	POP-Am	80
				Polyurethane	5
8.	H	Me	10	POP-Am	54
				Polyurethane	Trace

The porous polymer, POP-Am is found privileged to express catalytic role as it contains extended π- conjugation propagated through carboxamide linkage that stabilizes the free radicals generated by the breakdown of TBHP to higher extent. Thus, the presence of conjugated π- cloud in POP-Am plays an important role in the oxidation reactions with better yield. To revalidate the influence of π-cloud and carboxamide linkage in governing the rate of reaction the aforesaid reaction was conducted employing other carboxamide monomeric unit viz. *N*-phenyl-benzamide (I) and trimeric unit viz. $N^1N^3N^5$-triphenylbenzene-1,3,5-tricarboxamide (II) as catalyst. No reaction progress was detected in presence of I. Whereas, trace amount of corresponding benzaldehydes with no by-products have been isolated upon employing II (Table 2.4). Thus, it is true that the trend would lead to remarkable yield with 100 % selectivity for POP-Am which envisages vital role played by the active centres, i.e. carboxamide and π-conjugation in initiating and propagating the reaction.

Table 2.4 Catalytic activity of amide functionality monomeric units with TBHP as oxidant for the oxidation of benzyl alcohols under identical conditions in Table 2.1

Entry	R_1	R_2	Time (h)	Monomers	Yield (%)
1.	H	H	14	I	ND
				II	2
2.	Cl	H	14	I	ND
				II	1
3	Br	H	14	I	ND
				II	Trace
4.	NO_2	H	14	I	ND
				II	~ 2
5.	Me	H	14	I	ND
				II	Trace
6.	OMe	H	14	I	ND
				II	~ 2
7.	H	Phenyl	10	I	ND
				II	5
8.	H	Me	10	I	ND
				II	1

*ND: Not detected in GC-MS.

2.3.4 Catalyst reusability test

The reusability of a catalyst in heterogeneous catalytic reactions is an important parameter. As a result the reusability of POP-Am in accomplishing the oxidation of benzyl alcohols was verified with *p*-methyl benzyl alcohol substrate (Figure 2.8a). It has been observed that it could be effectively and efficiently used up to fourth cycle without much loss in yield % to afford corresponding benzaldehyde with selectivity. The reused POP-Am material is further analyzed by FT-IR and PXRD techniques (Figure 2.8b). The identical PXRD pattern of POP-Am material used up to fourth cycle upon comparison with that of afresh catalyst pattern reveals that the structural integrity of the POP-Am is preserved even after the catalytic cycle.

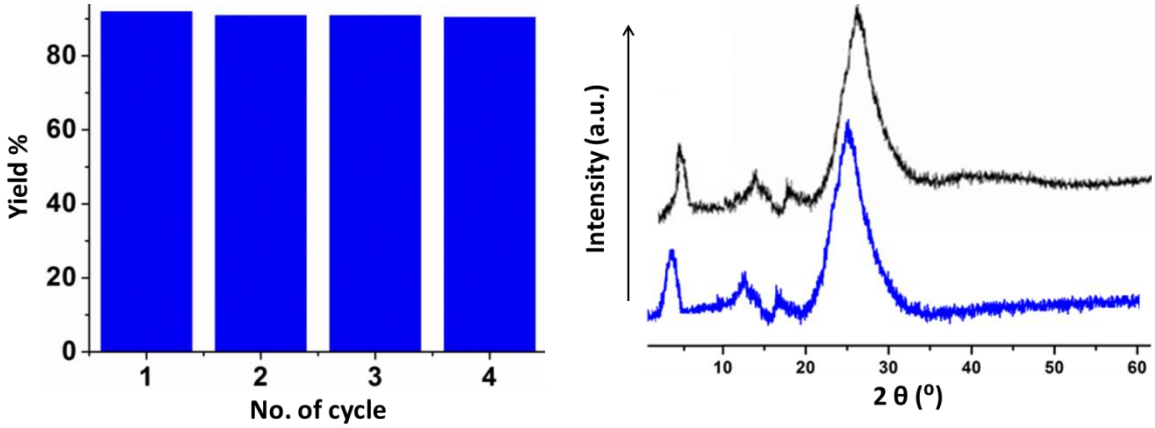

(a) (b)

Figure 2.8 Bar diagram representing the yield % of *p*-methyl benzaldehyde in the catalytic reusability of POP-Am (a) and identical PXRD pattern (b) of POP-Am after 4th cycle (blue) to that of the as synthesized pattern (black) displays the stability of POP-Am.

2.3.5 Reaction mechanism study

In order to understand the role of POP-Am in initializing the reaction via the formation of free radicals, DFT computation is performed on a small unit of the POP-Am. Since the calculation was performed for a small section of the whole polymer the measurement of energy barriers involved in the related transition states is refrained. Initially, the theoretical study was accomplished considering H_2O_2 as the oxidant. All plausible interactions existing between the catalyst, oxidant and the reactant molecules are revealed by geometric optimizations. The −OH group of the oxidant first interacted with C=O of amide group of the catalyst via strong O−H···O hydrogen bonding ($C{=}O_{catalyst}\cdots HO_{oxidant}$ is 1.70Å & 1.84Å; Figure 2.9), thereby weakening peroxide linkages. The −OH groups also interacted with the π-cloud via directional O−H···π interaction stabilizing radicals on the catalyst surface.

Once the alcohol moiety comes in close contact with the catalyst, probably the peroxide unit gets detached from the catalyst surface and interacts with the benzyl alcohol (Figure 2.9C). At this point the peroxide unit possibly dissociates into two hydroxyl radicals. The OH radical finally abstracts one methylene proton of benzyl alcohol. While the second radical involved in abstracting the alcoholic OH proton led selective formation of benzaldehyde with the liberation of two water molecules (Figure 2.9D).

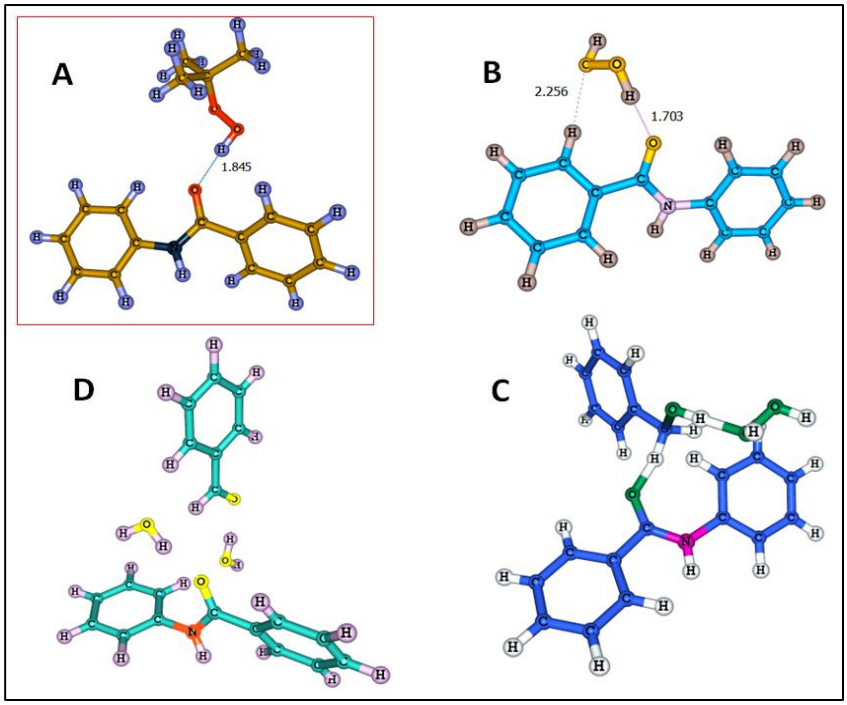

Figure 2.9 Plausible interactions between catalyst, oxidant and reactant molecules during catalytic oxidation process. (A) POP-Am + TBHP, (B) POP-Am + H_2O_2, (C) POP-Am + H_2O_2 + benzyl alcohol, (D) product formation with the liberation of 2 waters.

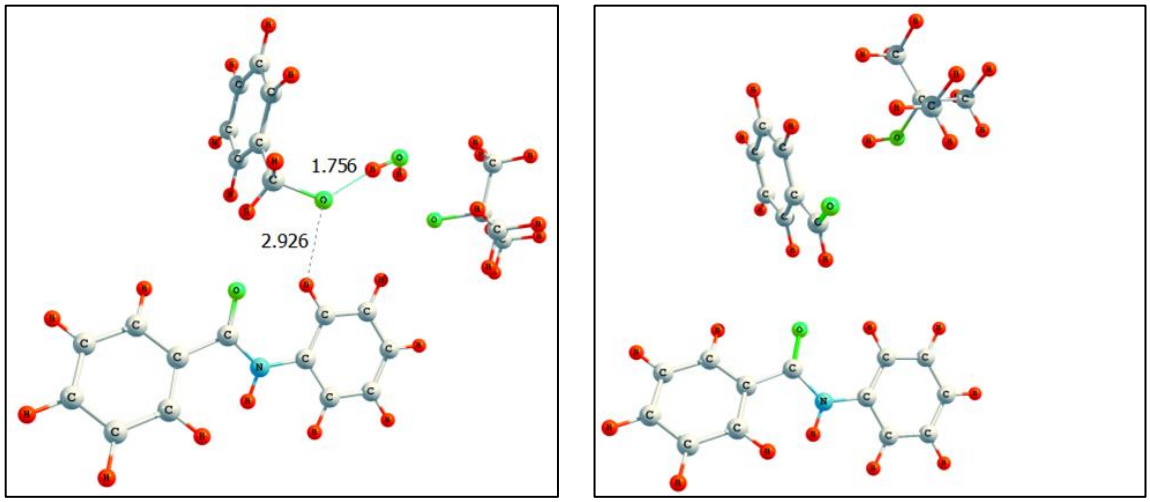

(a) (b)

Figure 2.10 Stepwise formation of benzaldehyde from benzyl alcohol in presence of TBHP supported by POP-Am as catalyst.

Alike calculation was performed for TBHP to understand the reaction mechanism. The TBHP molecule also acts in a similar manner. The stepwise decomposition of TBHP and its involvement in the abstraction of H from benzyl alcohol is shown in Figure 2.10. As the benzyl alcohol unit comes into play the TBHP moiety moves apart from the catalytic surface and allows the benzyl alcohol unit to interact to the catalyst surface *via* C–H···O

interaction. During this process the alcoholic proton of benzyl alcohol will be abstracted by TBHP forming two free radicals [Ar-$CH_2O^{\bullet}$ and $(CH_3)_3C\text{-}O^{\bullet}$] and a H_2O molecule. Ar-$CH_2O^{\bullet}$ free radical will get stabilized by weak C–H···O interaction (2.92Å) with POP-Am as shown in Figure 2.10a. In the subsequent step $(CH_3)_3C\text{-}O^{\bullet}$ radical will abstract one methylene H from benzyl alcohol forming benzaldehyde, and $(CH_3)_3COH$ (Figure 2.10b).

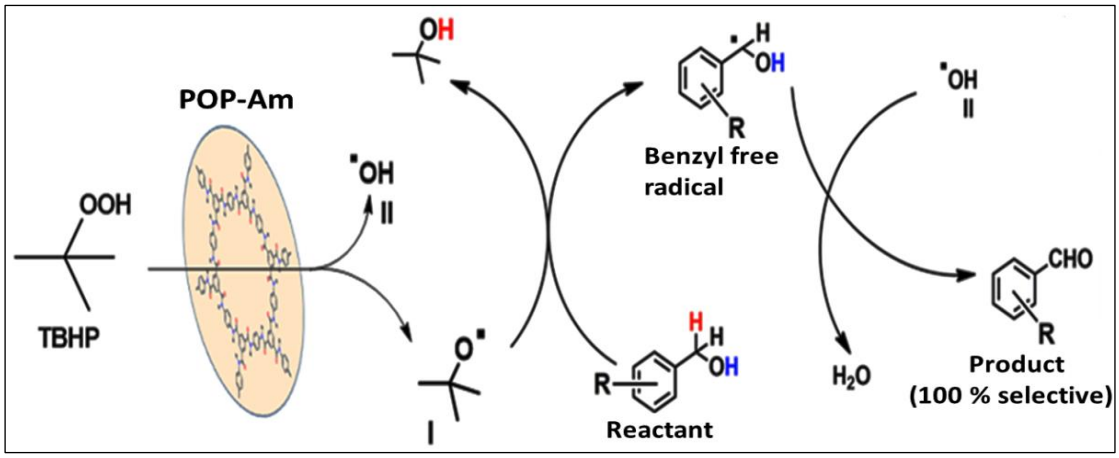

Scheme 2.5 Proposed free radical mechanism for the selective oxidation of benzyl alcohols to benzaldehydes using POP-Am as organocatalyst.

A trace amount of yield was observed when the reaction was performed in presence of H_2O_2. While in presence of TBHP, the selectivity goes up to 100% with moderate to excellent yield and no by-products. Thus, in order to substantiate this fact, the interaction energies were calculated for both the cases (Figure 2.9A and Figure 2.9B). Interaction energy for H_2O_2 + catalyst system was found to be highly positive (+127.5 $kcalmol^{-1}$); while for TBHP + catalyst system it was −61.5 $kcalmol^{-1}$ attributed preferred interaction of catalyst with TBHP. Hygroscopic environment inside pore dimension of POP-Am could contribute for stronger interactions of H_2O_2 with water rather than the catalyst. Large pore dimension also facilitated easy diffusion of H_2O_2 without being adsorbed on the surface and thereby reduces its activity. While in case of TBHP, the bulkier methyl group restricts its free diffusion and thereby it gets attached to the surface of the catalyst allowing the catalytic oxidation process to carry on. An important observation that has been made from the theoretical calculation is that dissociation of hydrogen peroxide and its involvement in proton abstraction seemed to be highly simultaneous. While in case of TBHP it proceeds in a stepwise manner. It was clear from the theoretical calculation that in presence of TBHP the intermediate species find some time to get stabilized and thus

induce high selectivity towards the product. Also the plausible π···π interactions between the product aldehyde and the catalyst surface could restrict its further oxidation to corresponding acid emphasizing lavish selectivity. Based on theoretical and experimental study a free radical mechanism of the oxidation reaction has been proposed and is depicted schematically in Scheme 2.5.

2.4 Summary

In this chapter, a new 2D POP with amide linkage in its framework comprising of π-electronic cloud propagated by carboxamide functionality is reported. This highly stable polymer exhibits continuous conjugation of *π*-electronic system is confirmed by solid state UV-Vis DR spectroscopy. Manifested by extremely low band gap of the conjugated *π*-cloud, the mesoporous polymeric network, POP-Am with tuned pore environment promotes selective oxidation of benzyl alcohols to the corresponding benzaldehydes. Improve in catalytic activity of the polymer is influenced by the hydrogen bonding and π···interactions between the reactants and the polymeric surface. It is anticipated that such organic molecular framework material stimulates their applicability to a broad range of catalytic applications that displays heaps of advantageous features. This is one of the rare cases of any organic polymer material acting as an outstanding organic catalyst with no metal add-ons.

2.5 Experimental

2.5.1 Materials

All chemicals and reagents utilized in the experiments were brought from commercial sources and used as received without further purification. 1,3,5-benzenetricarbonyl trichloride and *p*-pheneylenediammine are brought from Alfa Aesar. Tetrahydrofuran (THF) and triethylamine (TEA) were purchased from Sigma Aldrich. The benzyl alcohols were imported from Himedia and the solvents employed are purchased from Merck. All chemicals in the reactions are used as received. TLC silica gel F254 250 μm precoated-plates are brought from Merck.

2.5.2 Synthetic procedure for amide linked porous polymeric network (POP-Am)

A two neck round bottom flask was placed in ice cool condition and charged with *p*-phenylenediammine (1.5 mmol) solution in 5ml dry THF and added an excess amount of triethyl amine (TEA). Added to it 1,3,5-benzenetricarbonyl trichloride (1 mmol) solution

in 2mL THF over a period of 2 h maintaining the temperature at 0 °C. The mixture was kept in continuous stirring for another 12 h under inert atmosphere at room temperature. The precipitate was filtered using vacuum filtration and further purified by solvent washing with acetone in which both the starting moieties are soluble whereas the desired porous material (POP-Am) is insoluble.

2.5.3 Characterization/Instrumentation

2.5.3.1 FT-IR spectroscopy

FT-IR spectra were recorded in the frequency range of 400–4000 cm^{-1} in Perkin Elmer spectrophotometer. Approximately 1 mg of the sample to be recorded was ground with 100 mg of dry KBr, pressed the mixture by hydraulic pressure to afford the suitable pellet and the IR spectrum for the pellet was recorded.

2.5.3.2 Thermogravimetric (TGA) analysis

TGA analysis reveals the thermal stability of a material and the inclusion of any guest molecules in it. The analysis was performed on Schimadzu 60 thermal analyzer. The sample to be analyzed was initially dried and recorded the TGA thermogram for approximately 10 mg of the dry sample at heating rate of 10 °C min^{-1} under the continuous nitrogen flow.

2.5.3.3 Powder X-ray diffraction (PXRD) analysis

PXRD patterns were recorded on Bruker AXS (D8 FOCUS) using Cu Kα (λ = 1.542 Å) radiation with 2θ ranging from 10°– 60° (step size 0.01°) at the rate of 1° min^{-1}. The sample whose PXRD pattern is to be recorded was initially vacuum dried. Approximately 50 mg of vacuum dried sample was ground to fine powder and recorded PXRD pattern.

2.5.3.4 NMR spectroscopy

Solid state NMR (ssNMR) spectroscopy has been utilized for studying the chemical environment of the porous polymer as the material is insoluble in common NMR solvents. Solid state ^{13}C cross polarizing magic angle spinning (^{13}C CP-MAS) NMR data was recorded in Jeol 400 MHz spectrophotometer with spin rate of 5000 Hz employing 4 nm MAS probe. Nearly 400 mg of vacuum dried ground fine powder was taken and recorded ss-NMR. Whereas, the liquid NMR using deuterated NMR solvents, namely-

dimethyl sulfoxide-d6 and chloroform-d1 was recorded in JEOL 400 MHz spectrophotometer.

2.5.3.5 UV-vis spectroscopy

The UV-vis spectra of the solid samples were recorded in UV-Vis spectrophotometer made by Schimadzu in the range 200–800 nm.

2.5.3.6 BET surface area analysis

The adsorption isotherm, porosity and rigidity of the porous polymeric material were recorded in Brunauer–Emmett–Teller (BET) surface area analyzer made by Quantchrome Novawin (Version 10.01). Ultra high purity nitrogen (99.999% pure) was considered for the measurement and the temperature during the process was controlled via refrigerated bath of liquid nitrogen (77 K). Prior to N_2 adsorption-desorption isotherm measurement the sample was degasified at 250 ºC for 4 h.

2.5.3.7 Electron microscopy

Scanning electron microscope (SEM) images were recorded in JEOL JSM 6390 to examine the surface morphology of the material. The sample was initially coated with gold coating and recorded the morphology at an accelerating voltage of 200 kV. Transmission electron microscope (TEM) images were recorded in JEOL JEM 2100 at the accelerating voltage of 200 kV. The samples are initially dispersed at methanol by ultrasonication method, placed as thinly as possible to the carbon coated TEM grid, allowed to dry and recorded the images.

2.5.3.8 Gas chromatography-mass spectrometry (GC-MS) technique

The GC-MS (Schimadzu) is used to verify the progress of the oxidation reaction and to characterize the reaction mixture. About 100 µL of the reaction mixture was retrieved and placed in the solution mixture of ethyl acetate and water. The mixture was centrifuged and collected the organic layer which was dried over anhydrous sodium sulfate. Thus collected reaction mixture was further diluted by HPLC grade ethyl acetate and injected 10 µL of it into the GC-MS column.

2.5.3.9 Computational details

The density functional theory (DFT) [51] calculations were performed using Gaussian09 programme [52] to understand the mechanistic pathway of oxidation reactions. The functional used in this study was the B3LYP, consisting of a hybrid exchange functional as defined by Becke's three-parameter equation [53] and the Lee-Yang-Parr correlation functional [54]. The ground state geometry was obtained in the gas phase by full geometry optimization. And the optimum structure located as stationary point on the potential energy surface was verified by the absence of imaginary frequencies. The basis set used in this study was 6-311++G(d,p). DMol3 in Material Studio 7.0 package has been utilized to optimize 2.2 nm radius ring structure.

2.6 References

[1] Côté, A. P., Benin, A. I., Ockwig, N. W., O´keeffe, M., Matzger, A. J. and Yaghi, O. M. Porous, crystalline, covalent organic frameworks. *Science*, 310(5751):1166-1170, 2005.

[2] Feng, X., Ding, X. and Jiang, D. Covalent organic frameworks. *Chemical Society Reviews*, 41(18):6010-6022, 2012.

[3] Holden, D., Chong, S. Y., Chen, L., Jelfs, K. E., Hasell, T. and Cooper, A. I. Understanding static, dynamic and cooperative porosity in molecular materials. *Chemical Science*, 7(8):4875-4879, 2016.

[4] Chen, X., Addicoat, M., Irle, S., Nagai, A. and Jiang, D. Control of crystallinity and porosity of covalent organic frameworks by managing interlayer interactions based on self-complementary π-electronic force. *Journal of the American Chemical Society*, 135(2):546-549, 2013.

[5] Ma, H., Liu, B., Li, B., Zhang, L., Li, Y. G., Tan, H. Q., Zang, H. Y. and Zhu, G. Cationic covalent organic frameworks: a simple platform of anionic exchange for porosity tuning and proton conduction. *Journal of the American Chemical Society*, 138(18):5897-5903, 2016.

[6] Mendoza-Cortes, J. L., Goddard III, W. A., Furukawa, H. and Yaghi, O. M. A covalent organic framework that exceeds the DOE 2015 volumetric target for H_2 uptake at 298 K. *The Journal of Physical Chemistry Letters*, 3(18):2671-2675, 2012.

[7] Zhu, Y., Long, H. and Zhang, W. Imine-linked porous polymer frameworks with high small gas (H_2, CO_2, CH_4, C_2H_2) uptake and CO_2/N_2 selectivity. *Chemistry of Materials*, 25(9):1630-1635, 2013.

[8] Lu, W., Yuan, D., Zhao, D., Schilling, C. I., Plietzsch, O., Muller, T., Bräse, S., Guenther, J., Blümel, J., Krishna, R., Li, Z. and Zhou, H. C. Porous polymer networks: synthesis, porosity, and applications in gas storage/separation. *Chemistry of Materials*, 22(21):5964-5972, 2010.

[9] Hao, L., Ning, J., Luo, B., Wang, B., Zhang, Y., Tang, Z., Yang, J., Thomas, A. and Zhi, L. Structural evolution of 2D microporous covalent triazine-based framework toward the study of high-performance supercapacitors. *Journal of the American Chemical Society*, 137(1):219-225, 2014.

[10] Chandra, S., Kundu, T., Kandambeth, S., BabaRao, R., Marathe, Y., Kunjir, S. M. and Banerjee, R. Phosphoric acid loaded azo (−N=N−) based covalent organic framework for proton conduction. *Journal of the American Chemical Society*, 136(18):6570-6573, 2014.

[11] Furukawa, H. and Yaghi, O. M. Storage of hydrogen, methane, and carbon dioxide in highly porous covalent organic frameworks for clean energy applications. *Journal of the American Chemical Society*, 131(25):8875-8883, 2009.

[12] Yadav, R. K., Kumar, A., Park, N. J., Kong, K. J. and Baeg, J. O. A highly efficient covalent organic framework film photocatalyst for selective solar fuel production from CO_2. *Journal of Materials Chemistry A*, 4(24):9413-9418, 2016.

[13] Lee, J. S. M., Wu, T. H., Alston, B. M., Briggs, M. E., Hasell, T., Hu, C. C. and Cooper, A. I. Porosity-engineered carbons for supercapacitive energy storage using conjugated microporous polymer precursors. *Journal of Materials Chemistry A*, 4(20):7665-7673, 2016.

[14] Bhanja, P., Mishra, S., Manna, K., Saha, K. D. and Bhaumik, A. Porous polymer bearing polyphenolic organic building units as a chemotherapeutic agent for cancer treatment. *ACS Omega*, 3(1):529-535, 2018.

[15] Sun, Q., Fu, C. W., Aguila, B., Perman, J., Wang, S., Huang, H. Y., Xiao, F. S. and Ma, S. Pore environment control and enhanced performance of enzymes infiltrated in covalent organic frameworks. *Journal of the American Chemical Society*, 140(3):984-992, 2018.

[16] Xu, H., Gao, J. and Jiang, D. Stable, crystalline, porous, covalent organic frameworks as a platform for chiral organocatalysts. *Nature Chemistry*, 7(11):905-912, 2015.

[17] Chan-Thaw, C. E., Villa, A., Katekomol, P., Su, D., Thomas, A. and Prati, L. Covalent triazine framework as catalytic support for liquid phase reaction. *Nano Letters*, 10(2):537-541, 2010.

[18] Ding, S. Y., Gao, J., Wang, Q., Zhang, Y., Song, W.G., Su, C. Y. and Wang, W. Construction of covalent organic framework for catalysis: Pd/COF-LZU1 in Suzuki–Miyaura coupling reaction. *Journal of the American Chemical Society*, 133(49):19816-19822, 2011.

[19] Puthiaraj, P. and Pitchumani, K. Palladium nanoparticles supported on triazine functionalized mesoporous covalent organic polymers as efficient catalysts for Mizoroki–Heck cross coupling reaction. *Green Chemistry*, 16(9):4223-4233, 2014.

[20] Fang, Q., Gu, S., Zheng, J., Zhuang, Z., Qiu, S. and Yan, Y. 3D microporous base-functionalized covalent organic frameworks for size-selective catalysis. *Angewandte Chemie International Edition*, 53(11):2878-2882, 2014.

[21] Xu, H., Chen, X., Gao, J., Lin, J., Addicoat, M., Irle, S. and Jiang, D. Catalytic covalent organic frameworks via pore surface engineering. *Chemical Communications*, 50(11):1292-1294, 2014.

[22] Shinde, D. B., Kandambeth, S., Pachfule, P., Kumar, R. R. and Banerjee, R. Bifunctional covalent organic frameworks with two dimensional organocatalytic micropores. *Chemical Communications*, 51(2):310-313, 2015.

[23] Sun, Q., Aguila, B. and Ma, S. A bifunctional covalent organic framework as an efficient platform for cascade catalysis. *Materials Chemistry Frontiers*, 1(7):1310-1316, 2017.

[24] Pachfule, P., Kandambeth, S., Díaz, D. D. and Banerjee, R. Highly stable covalent organic framework–Au nanoparticles hybrids for enhanced activity for nitrophenol reduction. *Chemical Communications*, 50(24):3169-3172, 2014.

[25] Wu, Y., Xu, H., Chen, X., Gao, J. and Jiang, D. A π-electronic covalent organic framework catalyst: π-walls as catalytic beds for Diels–Alder reactions under ambient conditions. *Chemical Communications*, 51(50):10096-10098, 2015.

[26] Wang, C. A., Li, Y. W., Han, Y. F., Zhang, J. P., Wu, R. T. and He, G. F. The "bottom-up" construction of chiral porous organic polymers for heterogeneous asymmetric organocatalysis: MacMillan catalyst built-in nanoporous organic frameworks. *Polymer Chemistry*, 8(36):5561-5569, 2017.

[27] Lin, S., Diercks, C. S., Zhang, Y. B., Kornienko, N., Nichols, E. M., Zhao, Y., Paris, A. R., Kim, D., Yang, P., Yaghi, O. M. and Chang, C. J. Covalent organic frameworks comprising cobalt porphyrins for catalytic CO_2 reduction in water. *Science*, 349(6253):1208-1213, 2015.

[28] Zhi, Y., Shao, P., Feng, X., Xia, H., Zhang, Y., Shi, Z., Mu, Y. and Liu, X. Covalent organic frameworks: Efficient, metal-free, heterogeneous organocatalysts for chemical fixation of CO_2 under mild conditions. *Journal of Materials Chemistry A*, 6(2):374-382, 2018.

[29] Kaur, P., Hupp, J. T. and Nguyen, S. T. Porous organic polymers in catalysis: opportunities and challenges. *ACS Catalysis*, 1(7):819-835, 2011.

[30] Jing, L. P., Sun, J. S., Sun, F., Chen, P. and Zhu, G. Porous aromatic framework with mesopores as a platform for a super-efficient heterogeneous Pd-based organometallic catalysis. *Chemical Science*, 9(14):3523-3530, 2018.

[31] Fang, H., Sun, S., Liao, P., Hu, Y. and Zhang, J. Gold nanoparticles confined in imidazolium-based porous organic polymers to assemble a microfluidic reactor: Controllable growth and enhanced catalytic activity. *Journal of Materials Chemistry A*, 6(5):2115-2121, 2018.

[32] Dhanalaxmi, K., Singuru, R., Mondal, S., Bai, L., Reddy, B. M., Bhaumik, A. and Mondal, J. Magnetic nanohybrid decorated porous organic polymer: synergistic catalyst for high performance levulinic acid hydrogenation. *ACS Sustainable Chemistry & Engineering*, 5(1):1033-1045, 2016.

[33] Mondal, S., Singuru, R., Shit, S. C., Hayashi, T., Irle, S., Hijikata, Y., Mondal, J. and Bhaumik, A. Ruthenium nanoparticle-decorated porous organic network for direct hydrodeoxygenation of long-chain fatty acids to alkanes. *ACS Sustainable Chemistry & Engineering*, 6(2):1610-1619, 2018.

[34] Khatioda, R., Talukdar, D., Saikia, B., Bania, K. K. and Sarma, B. Constructing two dimensional amide porous polymer to promote selective oxidation reactions. *Catalysis Science & Technology*, 7(14):3143-3150, 2017.

[35] Corey, E. J. and Suggs, J. W. Pyridinium chlorochromate. An efficient reagent for oxidation of primary and secondary alcohols to carbonyl compounds. *Tetrahedron Letters*, 16(31):2647-2650, 1975.

[36] Omura, K., Sharma, A. K. and Swern, D. Dimethyl sulfoxide-trifluoroacetic anhydride. New reagent for oxidation of alcohols to carbonyls. *The Journal of Organic Chemistry*, 41(6):957-962, 1976.

[37] Meyer, S. D. and Schreiber, S. L. Acceleration of the Dess-Martin oxidation by water. *The Journal of Organic Chemistry*, 59(24):7549-7552, 1994.

[38] Liu, M., Fan, G., Yu, J., Yang, L. and Li, F. Defect-rich Ni–Ti layered double hydroxide as a highly efficient support for Au nanoparticles in base-free and solvent-free selective oxidation of benzyl alcohol. *Dalton Transactions*, 47(15):5226-5235, 2018.

[39] Mannel, D. S., King, J., Preger, Y., Ahmed, M. S., Root, T. W. and Stahl, S. S. Mechanistic insights into aerobic oxidative methyl esterification of primary alcohols with heterogeneous PdBiTe Catalysts. *ACS Catalysis*, 8(2):1038-1047, 2018.

[40] Ho, W. C., Chung, K., Ingram, A. J. and Waymouth, R. M. Pd-catalyzed aerobic oxidation reactions: strategies to increase catalyst lifetimes. *Journal of the American Chemical Society*, 140(2):748-757, 2018.

[41] Bolzan, G. R., Abarca, G., Gonçalves, W. D., Matos, C. F., Santos, M. J. and Dupont, J. Imprinted naked Pt nanoparticles on N-doped carbon supports: a synergistic effect between catalyst and support. *Chemistry–A European Journal*, 24(6):1365-1372, 2018.

[42] Patil, M. R., Kapdi, A. R. and Kumar, A. V. Recyclable supramolecular ruthenium catalyst for the selective aerobic oxidation of alcohols on water: application to total synthesis of brittonin. *ACS Sustainable Chemistry & Engineering*, 6(3):3264-3278, 2018.

[43] Li, M., Cárdenas-Lizana, F. and Keane, M. A. Combined catalytic action of supported Cu and Au in imine production from coupled benzyl alcohol and nitrobenzene reactions. *Applied Catalysis A: General*, 557:145-153, 2018.

[44] Bhat, G. A., Rajendran, A. and Murugavel, R. Dinuclear manganese(II), Cobalt(II), and nickel(II) aryl phosphates incorporating 4′-chloro-2,2′:6′,2″-terpyridine coligands – efficient catalysts for alcohol oxidation. *European Journal of Inorganic Chemistry*, 2018(6):795-804, 2018.

[45] Wang, X., Liu, R., Jin, Y. and Liang, X. TEMPO/HCl/$NaNO_2$ catalyst: A transition-metal-free approach to efficient aerobic oxidation of alcohols to aldehydes and ketones under mild conditions. *Chemistry-A European Journal*, 14(9):2679-2685, 2008.

[46] Patel, M. A., Luo, F., Khoshi, M. R., Rabie, E., Zhang, Q., Flach, C. R., Mendelsohn, R., Garfunkel, E., Szostak, M. and He, H. P-doped porous carbon as metal free catalysts for selective aerobic oxidation with an unexpected mechanism. *ACS Nano*, 10(2):2305-2315, 2016.

[47] Long, J., Xie, X., Xu, J., Gu, Q., Chen, L. and Wang, X. nitrogen-doped graphene nanosheets as metal-free catalysts for aerobic selective oxidation of benzylic alcohols. *ACS Catalysis*, 2(4):622-631, 2012.

[48] Zečević, J., Gommes, C. J., Friedrich, H., de Jongh, P. E. and de Jong, K. P. Mesoporosity of zeolite Y: Quantitative three-dimensional study by image analysis of electron tomograms. *Angewandte Chemie International Edition*, 51(17):4213-4217, 2012.

[49] Delley, B. An all-electron numerical method for solving the local density functional for polyatomic molecules. *The Journal of Chemical Physics*, 92(1):508-517, 1990.

[50] Marrocchi, A., Facchetti, A., Lanari, D., Santoro, S. and Vaccaro, L. Click-chemistry approaches to π-conjugated polymers for organic electronics applications. *Chemical Science*, 7(10):6298-6308, 2016.

[51] Parr, R. G. and Yang, W. Density-functional theory of atoms and molecules. *Oxford University Press*, New York, 1989.

[52] Frisch, M. J., Trucks, G. W., Schlegel, H. B., Scuseria, G. E., Robb, M. A., Cheeseman, J. R., Scalmani, G., Barone, V., Mennucci, B., Petersson, G. A. and Nakatsuji, H. *Gaussian 09, Revision B. 01* (Wallingford, CT: Gaussian, Inc., 2010).

[53] Becke, A. D. Density-functional thermochemistry. III. The role of exact exchange. *The Journal of Chemical Physics*, 98(7):5648-5652, 1993.

[54] Lee, C., Yang, W. and Parr, R. G. Development of the colle-salvetti correlation-energy formula into a functional of the electron density. *Physical Review B*, 37(2):785-789, 1988.